Geological and textural characteristics as evidence for Irish-type mineralization in the Eastern Haft-Savaran deposit

Pouria Mahmoodi[1], Jan M. Peter[2], Abdorrahman Rajabi[3] & Ebrahim Rastad[1]

[1] *Department of Geology, Faculty of Basic Sciences, Tarbiat Modares University, Tehran 14115-175, Iran*

[2] *Geological Survey of Canada, 601 Booth Street, Ottawa, Ontario K1A 0E8, Canada*

[3] *School of Geology, College of Science, University of Tehran, Tehran 14155-6455, Iran*

Corresponding Author: Pouria Mahmoodi   airop1365@gmail.com

Geological and textural characteristics as evidence for Irish-type mineralization in the Eastern Haft-Savaran deposit

Pouria Mahmoodi[1], Jan M. Peter[2], Abdorrahman Rajabi[3] & Ebrahim Rastad[1]

[1] Department of Geology, Faculty of Basic Sciences, Tarbiat Modares University, Tehran 14115-175, Iran
[2] Geological Survey of Canada, 601 Booth Street, Ottawa, Ontario K1A 0E8, Canada
[3] School of Geology, College of Science, University of Tehran, Tehran 14155-6455, Iran

Abstract: The Eastern Haft-Savaran Zn-Pb-(Ba) deposit, located in the southeastern part of the Arak Mining District of the Malayer-Esfahan Metallogenic Belt, Iran, is hosted in the uppermost part of an early Cretaceous massive limestone unit that is capped by shale. The mineralization has a sheet-like geometry and is associated with intense dolomitization and silicification. The mineralization is mineralogically zoned: chalcopyrite-galena-pyrite-sphalerite-tetrahedrite occurs in the southern part of the deposit; sphalerite-galena-pyrite occurs in the central part of the deposit; and barite-galena-sphalerite-pyrite occurs in the northern part of the deposit. The thickest mineralization and most intense alteration are in the southern part of the deposit, associated with an aphyric rhyodacite flow containing minute euhedral barite crystals and Cu-bearing sulphides in vein/veinlets and disseminations, indicating this was the mineralizing fluid upflow site. Three hydrothermal mineralization stages are recognized. The first is mud lime sedimentation, framboidal pyrite, minute euhedral barite, sphalerite, galena and early dolomite. Minute euhedral barites are cut by microsparite formed by micrite recrystallization during diagenesis. First stage sphalerite and galena occur as inclusions in framboidal pyrite, and these were remobilized into inclusions in euhedral pyrite during recrystallization. The second (main) stage mineralization includes sphalerite, galena, chalcopyrite, tetrahedrite, pyrite and barite that with dolomite and quartz as gangue minerals replaced first stage mineralization and is associated with silicification and dolomitization. The third stage of mineralization comprises sphalerite and galena that is associated with dolomitization and calcitization. The occurrence of mineralization in an extensional back arc setting, massive limestone host rock, intense and pervasive host rock alteration, Fe-dolomite associated with main stage mineralization, the presence of mineralization load casts and minute euhedral barite, the remobilization of first stage of mineralization during diagenetic evolution of framboidal pyrite to euhedral pyrite, and timing of mineralization during early diagenesis of mud lime collectively indicate the Eastern Haft-Savaran deposit can be classified as an Irish-type deposit.

Keywords: Eastern Haft-Savaran deposit; Early Cretaceous; euhedral barite; framboidal pyrite; early diagenetic mineralization; sub-seafloor replacement, Irish-type deposit

Introduction

Sediment-hosted Zn-Pb deposits are the main source of the world's Zn and Pb (Singer, 1995). Two of the most important sediment-hosted Zn-Pb deposit types are SedEx ("sedimentary exhalative"), also termed "clastic-dominated" (Leach *et al.,* 2010) and Mississippi Valley-type (MVT) deposits (Leach *et al.,* 2005). These deposit types provide 48% and 52% of Zn and Pb of the world, respectively (Singer, 1995). Another important sediment-hosted Zn-Pb deposit type is Irish-type deposits that are hosted by carbonates and show transitional characteristics between SedEx deposits and MVT deposits (Wilkinson, 2014). SedEx deposits form syn-diagenetically in clastic-dominant sequences and extensional settings, whereas MVT deposits form epigenetically in carbonate dominant sequences and compressional, and orogenic settings (Leach *et*

al., 2010). Irish-type deposits, however, occur in extensional settings within non-argillaceous carbonate rock in transgressive sequences (e.g., Lower Carboniferous shallow sea limestone covering late Devonian terrestrial red bed sandstone) and their relative timing is thought to be syn-diagenetic (i.e., similar to SedEx deposits). The Malayer-Esfahan Metallogenic Belt is a NW-SE trending, 400km by 100km wide metallotect located in the central portion of the Sanandaj-Sirjan Zone (Fig. 1A), that contains six Zn-Pb districts: 1) Esfahan, 2) Tiran, 3) Golpaygan, 4) Aligoodarz, 5) Arak and 6) Malayer (Fig. 1B). The Arak Mining District is the largest and most prolific Zn-Pb-(Ba) mining district in Iran (comprising 15 Zn-Pb ore deposits); it is NW-SE trending, 65 km long by 15 km wide, and is situated in the central part of the Malayer-Esfahan Metallogenic Belt (Momenzadeh, 1976; Rajabi *et al.*, 2012) (Fig. 1B). The ore deposits in the Arak Mining District
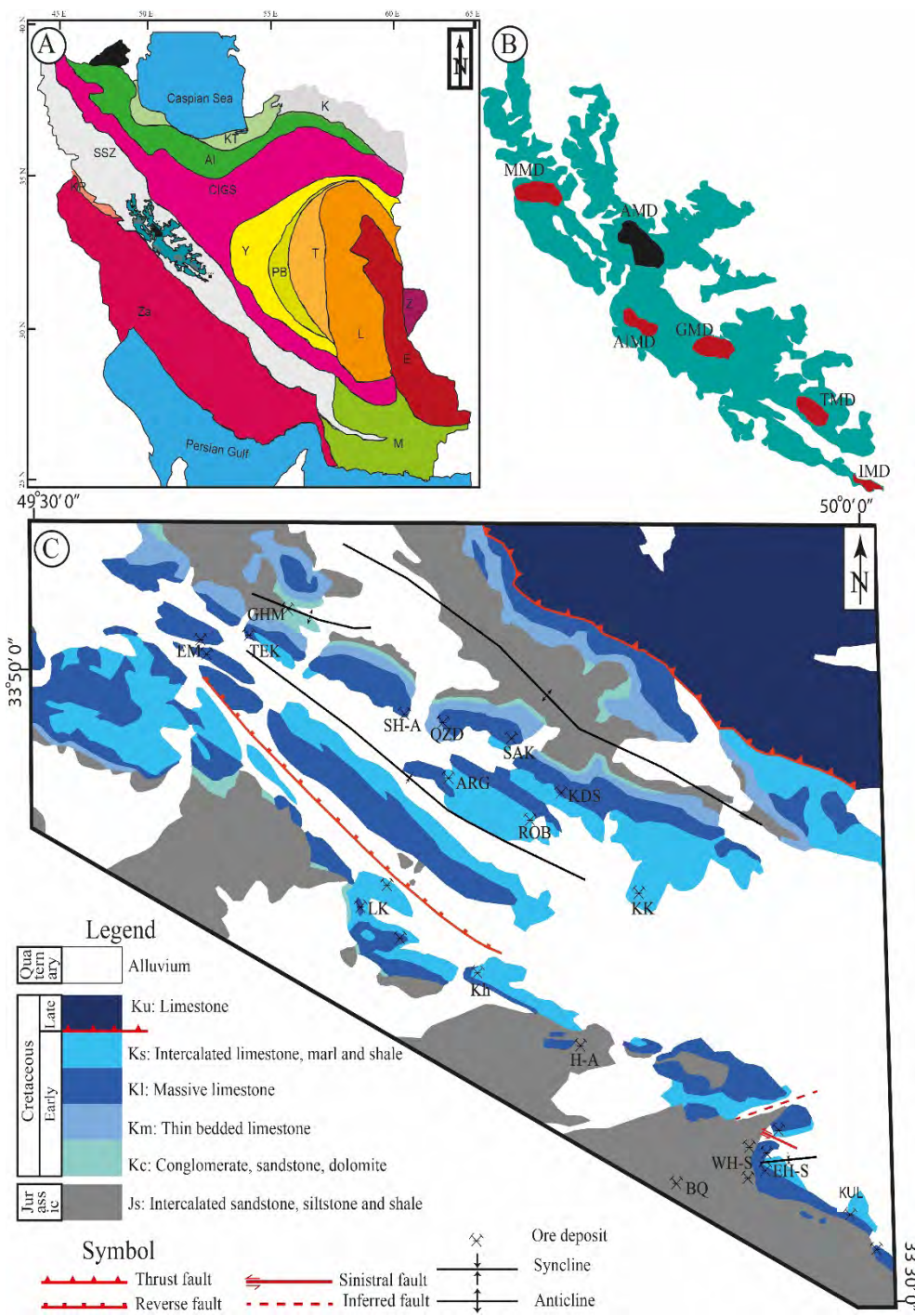
Figure 1 *–**A**) (inset) map of structural zones of Iran (Aghanabati, 2004); Al, Alborz ranges; CIGSZ, Central Iranian Geological and Structural Zone; E, East Iran ranges; K, Kopeh-Dagh; KR, Kermanshah Radiolarites subzone; KT, Khazar-Talesh- Ziveh structural zone; L, Lut block; M, Makran zone; O, ophiolite belts; PB, Posht-e Badam block; SSZ, Sanandaj-Sirjan zone; T, Tabas block; TM, tertiary magmatic rocks; UD, Urumieh-Dokhtar magmatic arc; Y, Yazd block; Z, Zabol area; Za, Zagros ranges. Modified after Aghanabati (2004).*

B) *Simplified map of Malayer-Esfahan metallogenic belt which contains 6 mining districts. IMD (Momenzadeh, 1976): Irankuh Mining District; TMD: Tiran Mining District; GMD: Golpaygan Mining District; AlMD: Aligodarz Mining District; AMD: Arak Mining District; MMD: Malayer Mining District.*

C) *Simplified geological map of the southern part of the Arak region in the Malayer-Esfahan metallogenic belt. Deposit name abbreviations are as follows: WH-S: Western Haft-Savaran, EH-S: Eastern Haft-Savaran, HA: Hossein-Abad- Em: Emarat, Baq: Baba-Qolleh, KDO: Kouh-Dom-Siyah, Kh: Khan-Abad, Ko: Kouh-Kolangeh, Kol: Kolisheh, Sh: Shams-Abad, La: Lakan, Ro: Robat, Sa: Saki, Te: Tekiyeh.*

are hosted in: 1) Jurassic shale, siltstone and sandstone, 2) early Cretaceous conglomerate, and 3) early Cretaceous massive limestone (Fig. 1C). The Eastern Haft-Savaran deposit, located in the southeastern part of the Arak Mining District, has a total geological resource of 2 Mt grading 3 wt.% Zn and 2 wt.% Pb.

Some researchers have classified the early Cretaceous clastic-carbonate-hosted mineralization in the Malayer-Esfahan Metallogenic Belt as MVT deposits that formed epigenetically (Hosseini-Dinani *et al.,* 2015; Hosseini-Dinani & Aftabi, 2016; Karimpour & Sadeghi, 2018; Nejadhadad *et al.,* 2018). However, others favor a synsedimentary to syndiagenetic origin (Yarmohammadi *et al.,* 2016; Boveiri *Konari et al.,* 2017; Boveiri Konari & Rastad, 2018; Rajabi *et al.,* 2019; Maanijou *et al.*, 2020). The Emarat Zn-Pb deposit in the northwestern part of the Arak Mining District was classified as an MVT deposit by Ehya *et al.* (2010) based on S and Pb isotopic data for hydrothermal sulphide minerals, whereas the Shams-Abad Fe-Mn-(Pb) deposit in the central part of the Arak Mining District was classified as a synsedimentary seafloor hydrothermal deposit (Ehya & Marbouti, 2021). Based on geological and textural characteristics, the Robat Zn-Pb-Ba deposit was classified as an Irish-type deposit by Niroomand *et al.* (2019). That two deposits within the same stratigraphic host rocks and 12 kilometers apart (Fig. 1C) are classified as different deposit types poses a conundrum.

Herein, we report on the geological, structural, textural and mineralogical characteristics of mineralization and host rock alteration of the Eastern Haft-Savaran deposit to understand formational processes and conditions. We focus on paragenesis, mineral chemistry of different dolomite generations, lithological characteristics that control mineralization, and deposit type classification.

Tectonostratigraphy

The subduction of the Neo-Tethys Ocean beneath the Sanandaj-Sirjan Zone caused extension that was induced by slab roll-back in the Sanandaj-Sirjan Zone and caused the opening of the Malayer-Esfahan super basin back-arc rift (Shahabpour, 2005; Bagheri & Stampfli, 2008; Moghadam *et al.,* 2009; Mohajjel & Fergusson, 2014). Extension in the Sanandaj-Sirjan Zone and in the Continental Iranian Geological Structural Zone commenced in the Late Jurassic and again in the Early Cretaceous after uplift in the Sanandaj-Sirjan Zone (Wilmsen et al., 2009), with initiation of opening of the back-arc basin, and deposition of a sequence of strata (base to top) from conglomerate to shale and limestone (Mohajjel & Fergusson, 2014; Wilmsen *et al.,* 2015). There are at least 150 Zn-Pb deposits and occurrences in the Malayer-Esfahan Metallogenic Belt. According to Rajabi *et al.* (2012), mineralization formed during early Cretaceous back-arc extension.

The Arak Mining District is a NW-SE trending syncline that in its central and marginal parts exposes Early Cretaceous and Jurassic strata (Fig. 1B). The Eastern Haft-Savaran deposit is located in the southeastern part of the Arak Mining District. The oldest rocks in the Eastern Haft-Savaran area are a succession of Jurassic dark gray to black sandstone, siltstone and shale that is overlain by early Cretaceous strata. The early Cretaceous sequence comprises (base to top): 1) regional dolomite

("Kc₃"); 2) Upper Baremian units, including massive Orbitolina-bearing limestone ("Kl"); 3) in the uppermost part of "Kl" is an aphanitic rhyodacite flow that contains rare alkali feldspar phenocrysts, and has a groundmass predominantly composed of quartz and alkali feldspar, together with accessory magnetite; and 4) Aptian units with intercalated shale, marl and limestone (Ks) (Momenzadeh, 1976; Mahmoodi *et al.,* 2018) (Fig. 2A, B).

Deposit geology

Mineralization in the Eastern Haft-Savaran deposit is stratabound and sheet-like (Fig. 2B) and replaces select beds in the host rock. Both the host rocks and mineralization have been folded, with fold axes striking NW-SE. Mineralization occurs within two discrete stratigraphic horizons (Fig. 2C). Mineralization (together with silicification and dolomitization alteration) occurs in the uppermost part of the "Kl" unit and in the limestone bed in the "Ks" unit (Fig. 2C). Due to the presence of these alteration styles, the mineralized horizon in uppermost "Kl", which is actively mined at present, is called Klsd.

Mineralization in the "Klsd" unit has an 800m strike length and averages 4 to 5m thick. Beneath this mineralized horizon, there is disseminated and uneconomic (not mined) mineralization in the "Kl" massive limestone, adjacent to an organic matter stylolite seam in limestone. Mineralization in "Klsd" can be divided into three discrete subzones (southern, central, and northern) based on sulphide mineral assemblages (Fig. 2B). The southern subzone, located near a probable reverse fault and outcropping volcanic rock, is characterized by a chalcopyrite-galena-pyrite-tetrahedrite-sphalerite assemblage (Fig. 2B). The central subzone is characterized by a sphalerite-pyrite-galena sulphide assemblage. The central subzone mineralization is banded and displays load casts, with galena and quartz loaded into limestone (Fig. 3A). The northern subzone of "Klsd" mineralization comprises vein-veinlet barite stratigraphically below a massive lens of barite (Fig. 3B) that also contains minor disseminated galena, sphalerite, and pyrite. The massive barite lens is farthest from the probable reverse fault and volcanic rocks (Fig. 2B).

Methodology

Samples were collected from drill cores and trenches for mineralogical studies. Least (un)deformed samples were selected for electron probe micro-analysis. Sixty-five polished thin sections were prepared of samples from the Eastern Haft-Savaran deposit to determine textures and paragenetic information, and a subset of 11 polished thin sections were selected for analysis of carbonate minerals by electron microprobe (2 from the northern part of the Eastern Haft-Savaran deposit; 2 from the southern part of the Eastern Haft-Savaran deposit; 3 from the central part of the Eastern Haft-Savaran deposit; 2 of weak hydrothermal alteration from the uppermost part of the Eastern Haft-Savaran deposit; and 2 of weak hydrothermal alteration from the middle part of the "Kl" unit of the Eastern Haft-Savaran deposit).

The polished thin sections were carbon coated and analyzed on a Camera SX100® electron microprobe at the Iranian Mineral Processing Research Center in Karaj. The detection limits for
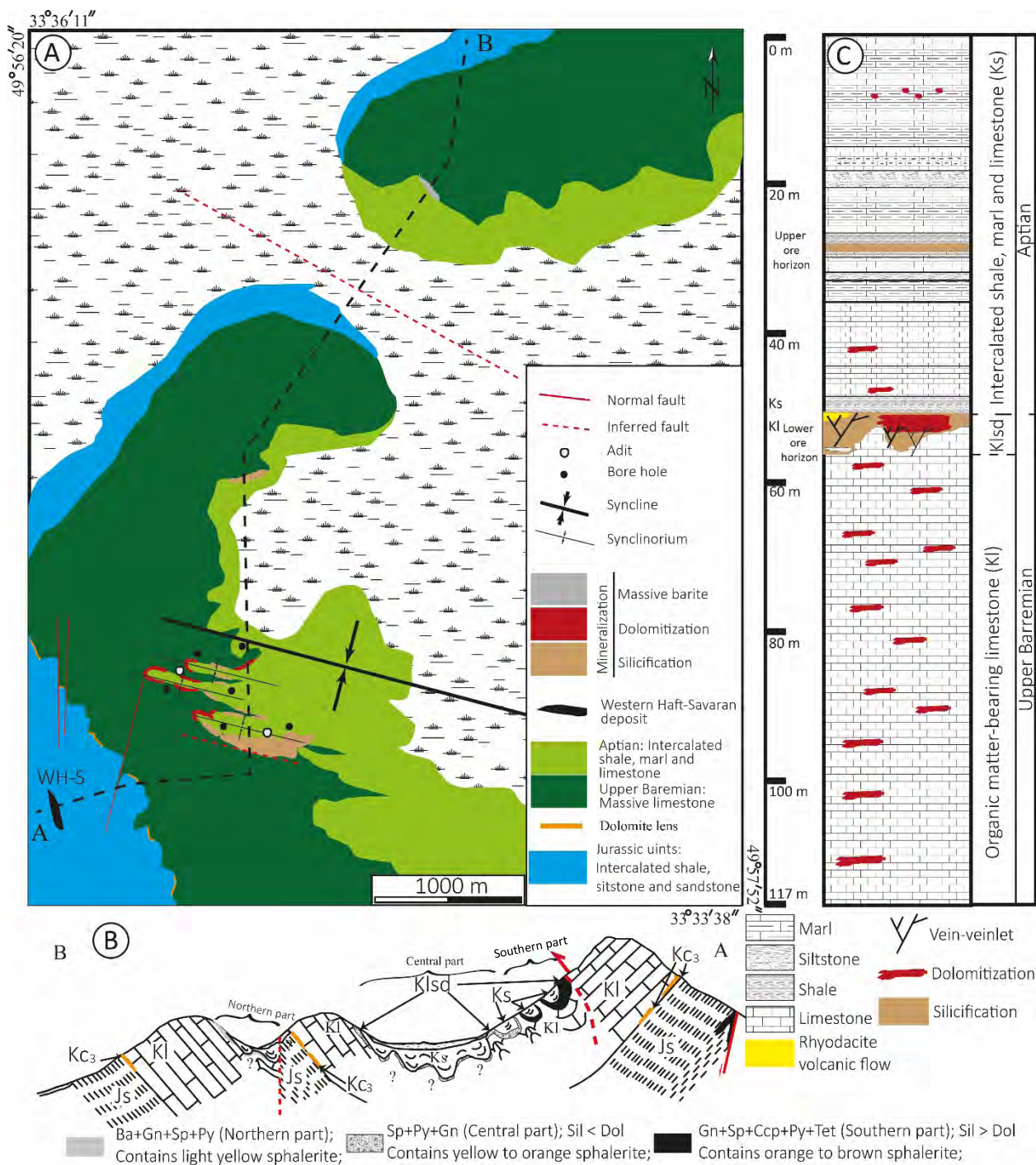
Figure 2 – *A) Geological map of the Eastern Haft-Savaran ore deposit. Line A-B shows location of cross-section of the deposit depicted in B. **B)** Schematic cross-section of the Eastern Haft-Savaran deposit. Mineralogical zoning of the Eastern Haft-Savaran deposit is also shown. **C)** Stratigraphic column of the Eastern Haft-Savaran deposit.*
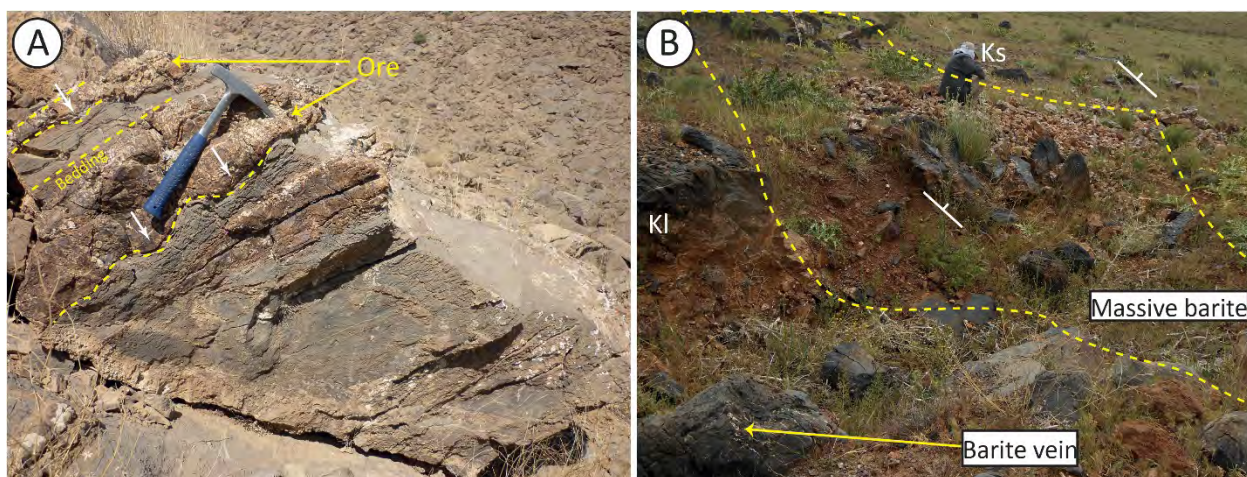
Figure 3 –*A) Weakly altered limestone in the central part of the Eastern Haft-Savaran deposit. Dashed yellow line shows bedding and white arrows indicate load casts of sulphide mineralization and hydrothermal alteration in unconsolidated mud; stratigraphic younging is to the top left of the photograph. B) Massive barite lens at the Kl-Ks boundary. Baritic veins-veinlets stratigraphically below massive barite.*

major and minor elements are 0.05 wt.% and 0.01 wt.%, respectively. Operating conditions (electron beam, current, beam diameter and matrix correction) were 20 Kev, 20 nA, 3 μm and ZAF, respectively.

To determine the paragenetic sequence of carbonate alteration, polished thin sections were stained with alizarin red and potassium ferrocyanide, and a subset of samples (8 in total: 2 from the weakly altered central part of "Kl"; 2 from the weakly altered upper part of the "Kl"; 2 from the intensely altered central part; 2 from the southern part) of the Eastern Haft-Savaran deposit were studied by cathodoluminescence.

Paragenesis

Ore minerals in the Eastern Haft-Savaran deposit are: sphalerite, galena, chalcopyrite, tetrahedrite, bornite, chalcocite, and covellite. Gangue minerals are pyrite, barite, dolomite, calcite, quartz and minor sericite. Based on the mineralogy, mineral textures and crosscutting relationships, four mineralization stages are recognized in the Eastern Haft-Savaran deposit (Fig. 4).

Early mineralization stage

The first stage of mineralization is represented by barite (Brt^1), dolomite (Dol^1), pyrite (Py^1, $Py^{2a, b}$), galena (Gn^1) and sphalerite (Sp^1) (Fig. 4). The first mineralization stage can be divided into two substages. The first substage began with deposition of host lime mud as wackestone, together with sedimentary framboidal pyrite and organic matter (Fig. 4). The second substage occurs as minute euhedral barite, sub-seafloor framboidal pyrite, dolomitization and minor sphalerite and galena (Fig. 4). Brt^1 occurs as disseminations in Orbitolina fossils and in the matrix interstitial to fossil fragments (Fig. 5A). These minute euhedral barites within the fossils are cut by microsparite calcite and first-generation dolomite (Fig. 5B, C). Sphalerite and galena inclusions occur in the framboids (Fig. 5D), and within fractures in spongy pyrite and as microcrystals in euhedral pyrite. Spongy pyrite (Py^{2a}) and euhedral pyrite (Py^{2b}) occur in

and on framboidal pyrite in the second substage (Fig. 5D).

First generation dolomite (Dol^1) is fine-grained (1 to 25 μm), and subhedral to anhedral. This dolomite is colourless under plane-polarized light (Fig. 5A) and orange under cathodoluminescence (Fig. 6A). This dolomite replaces fine-grained, euhedral barite (in the uppermost part of "Kl"), and is associated with framboidal pyrite and organic matter, whereas Dol^1 in "Klsd" has replaced the groundmass and matrix interstitial to Orbitolina fossils. Characteristics of both these Dol^1 occurrences are similar, and the only difference is Dol^1 in the "Klsd" is more pervasive than Dol^1 in the central portion of Kl.

Main-stage mineralization

In this stage, mineralization occurs as disseminations, veins-veinlets, and abundant replacements. The main stage of mineralization is divided into two substages (Fig. 4): 1) dolomitization-sulphidization, and 2) sulphidization-silicification. The first substage began with formation of second-generation dolomite (Dol^2), whereas the second substage began with silicification (Fig. 4). Sphalerite, pyrite, galena, chalcopyrite, tetrahedrite and barite are ore minerals formed in this stage and they replaced framboidal pyrite (Fig. 6B). Chalcopyrite occurs both as discrete grains and as chalcopyrite diseased sphalerite (Fig. 6C) in the southern part of the Eastern Haft-Savaran deposit.

Second generation dolomite (Dol^2) is coarse-grained, and subhedral to euhedral. Dol^2 stains blue (Fig. 6D) and is black coloured (Fig. 6E) under cathodoluminescence. Second generation dolomitization occurs as vein-veinlets, and replacements of fossils and groundmass. Dolomite in the vein-veinlets and fossils is coarser grained than dolomite in host rock matrix interstitial to fossils. Relict vestiges of Dol^1 remain in places.

Late-stage mineralization

Late-stage mineralization in the Eastern Haft-Savaran deposit occurs as veinlets and pseudobreccias in Klsd that are composed of third generation dolomite (Dol^3) and calcite. The main
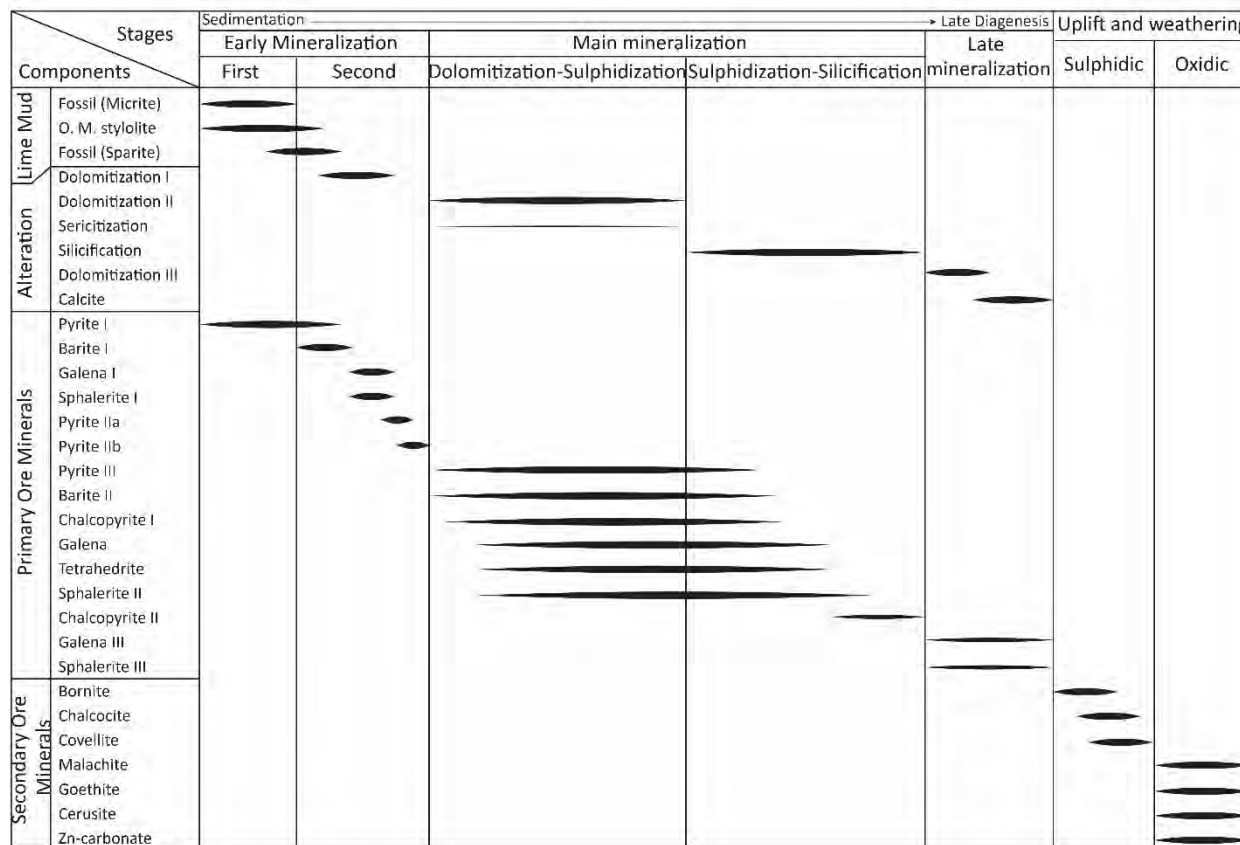
Figure 4 – *Paragenetic sequence of the Eastern Haft-Savaran deposit, as determined by microscopic study.*

minerals in this stage are calcite, Dol³, and minor Gn³ and Sp³ (Fig. 6F). The calcite and Dol³ crosscut and brecciate Dol¹, Dol², and quartz. Dol3 occurs as veinlets and as matrix that supports pseudobreccia fragments. Third generation carbonatization occurs as anhedral medium-grained dolomite (Dol³) and calcite (Cal) veinlets that crosscut and brecciate Dol2 (Fig. 6E). Dol³ is colourless and unreceptive to staining and is orange coloured under cathodoluminescence (Fig. 6E). Calcite in the veinlets stains red to purple and is yellow to red coloured under cathodoluminescence (Fig. 6E).

Uplift and weathering stage

Bornite, chalcocite, covellite, Zn-carbonate, cerussite, malachite and goethite formed from primary sulphide minerals during uplift, erosion and oxidative weathering.

Carbonate composition

The different generations of dolomite in the Eastern Haft-Savaran deposit are distinguished via staining and cathodoluminescence. The abundances of the four major cations (Fe, Mn, Ca and Mg) for each dolomite generation are given in Table 1 along with results for Zn, Pb and Cu. Second generation dolomite (Dol²) has the highest Fe (7.51 to 9.02 wt.%) and Mn (0.7 to 1.5 wt.%) contents whereas first generation dolomite (Dol¹) contains the lowest Fe (0.29 to 1.9 wt.%) and Mn (0.02 to 0.32 wt.%) (Table 1).

Discussion

Framboidal pyrite formation and evolution

In the eastern Haft-Savaran deposit, as in many sedimentary environments, there are large and well-developed pyrite framboids. In the Eastern Haft-Savaran deposit, sphalerite and galena occur as inclusions in framboidal pyrite. The microcrystalline sphalerite and galena may have a hydrothermal source and were formed immediately after framboidal pyrite formation.

The uniform size of microcrystals in the framboids of the Eastern Haft-Savaran deposit indicate that the microcrystals in any one framboid nucleated simultaneously (Wilkin *et al.,* 1996; Wilkin & Barnes, 1997). Accumulation of microcrystals should result in structures that extend from loose irregular aggregates to dense and compact spherical pyrite framboids and polyframboids (Wilkin & Barnes, 1997). Framboids have a mean diameter range of 6 to 10 μm and occur in association with crystalline pyrite and their size range indicates formation under dysoxic (partial oxygen restriction) conditions in pore fluids below the seafloor (Wilkin *et al.,* 1996; Wilkin *et al.,* 1997; Wignall & Newton, 1998; Bond & Wignall, 2010; Núñez-Useche *et al.,* 2016).

Diagenetic processes likely were important for formation and evolution of framboidal pyrite. Most framboidal pyrites
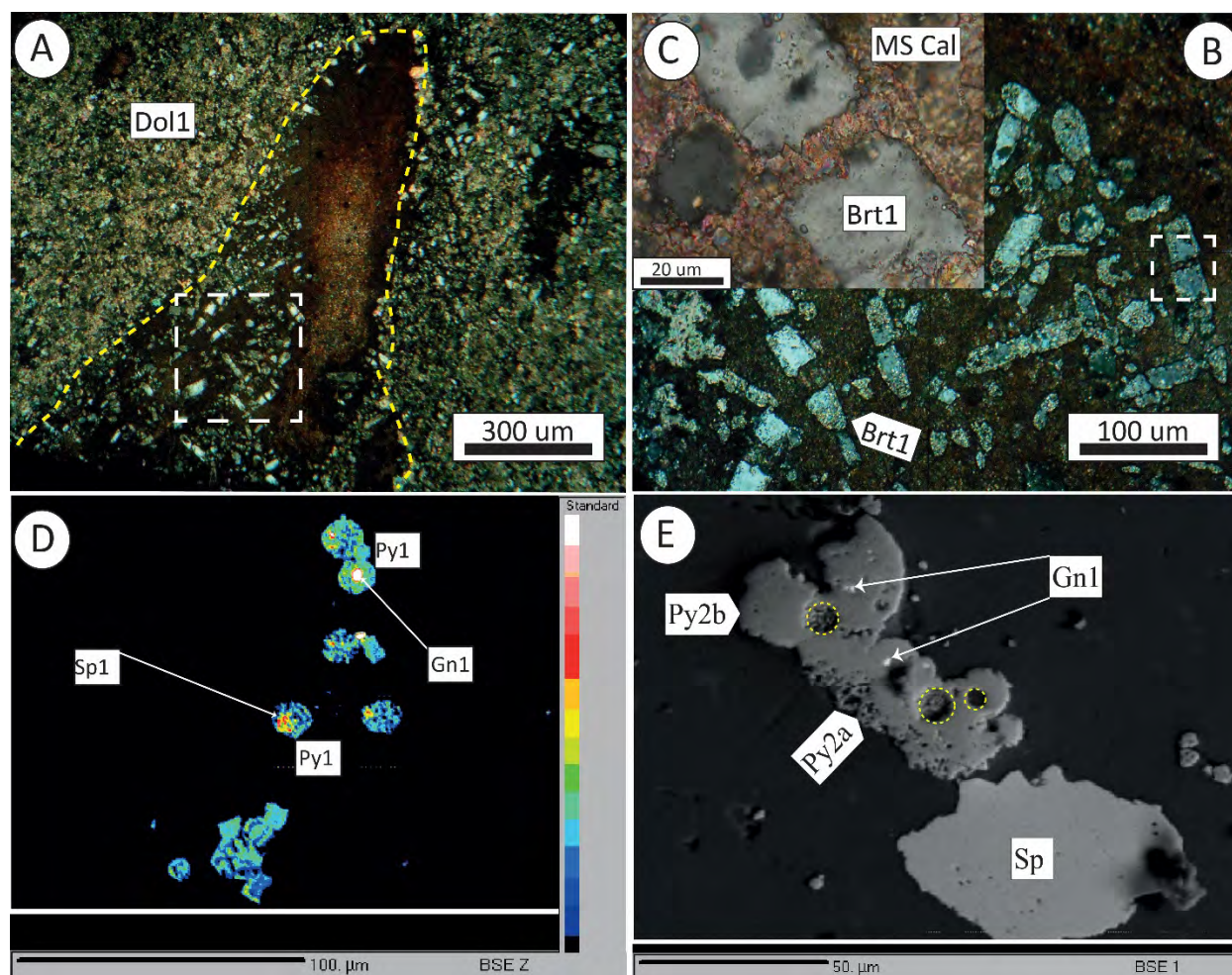
Figure 5 : *A) Plane-polarized light photomicrograph of weakly altered area in the central part of the Eastern Haft-Savaran deposit that shows Orbitolina fossils, first generation barite and first-generation dolomite. This polished thin section has been stained with alizarin red and potassium ferrocyanide, and Orbitolina fossils are coloured red and first-generation dolomites are colourless. Euhedral disseminated fine-grained barite is also present in the groundmass of the sample between fossils. Yellow dashed line outlines an Orbitolina fossil. Dashed white box shows region of "B". B) Cross-polarized light photomicrograph of dolomitized (first generation dolomite) minute euhedral barite in the Orbitolina fossil cut by calcite. Outlined white box shows region of "C". C) Cross-polarized light photomicrograph of minute euhedral barite cut by microsparite calcite in the fossil. D) Coloured BSE image of poly-framboidal pyrite from low-grade mineralization in uppermost Kl. Bluish green is pyrite, galena is white, and first-generation dolomite is black. Red is either: 1) sphalerite (where red area is a discrete patch), or 2) substituted portion (if red portion forms a ring around galena (white colour)). E) BSE image of spongy pyrite with relict framboids (with negative relief), and fine galena crystals. Dol1: First generation dolomite; Py1: First generation pyrite (as framboidal); Sp1: First generation sphalerite; Gn1: First generation galena; Py2b: Euhedral second-generation pyrite; Py2a: Spongy second-generation pyrite; Brt1: First generation barite; MS Cal: Microsparite calcite.*

formed in the mud and were replaced partly or completely by sphalerite and galena. Relict pyrite framboids remain within spongy pyrite, and euhedral pyrite forms rims around spongy pyrite. Fine-grained galena and sphalerite occur as: 1) inclusions in this remnant framboidal pyrite, 2) microcrystals in micro-fractures in spongy pyrite, and 3) crystals in the euhedral pyrite crystallized from spongy pyrite. During this textural evolution, galena and sphalerite that incipiently replaced framboids were remobilized into micro-fractures in spongy pyrite. Collectively, the presence of galena and sphalerite in all these textures indicates that the introduction and emplacement of Pb-Zn mineralization in the Eastern Haft-Savaran deposit commenced during early diagenesis. As diagenesis progressed, pyrite evolved texturally from framboids to spongy pyrite to euhedral pyrite.

Mineralization characteristics and timing

The Emarat deposit in the northwestern part of the Arak Mining District is the best-known Zn-Pb deposit in the district. The Shams-Abad deposit located in the central part of the Arak Mining District is an Fe-Mn deposit that contains lenses of massive galena. Both the Emarat deposit and the Shams-Abad deposit are hosted by the same uppermost part of the massive limestone immediately below shale unit ("Klsd") that hosts the Eastern Haft-Savaran deposit. The Emarat deposit has been classified as an MVT deposit (Ehya *et al.,* 2010), whereas the Shams-Abad deposit has been classified as synsedimentary seafloor hydrothermal (Ehya & Marbouti, 2021). Classification of these two deposits with similar stratigraphic positions as different deposit types do not seem logical, and we believe
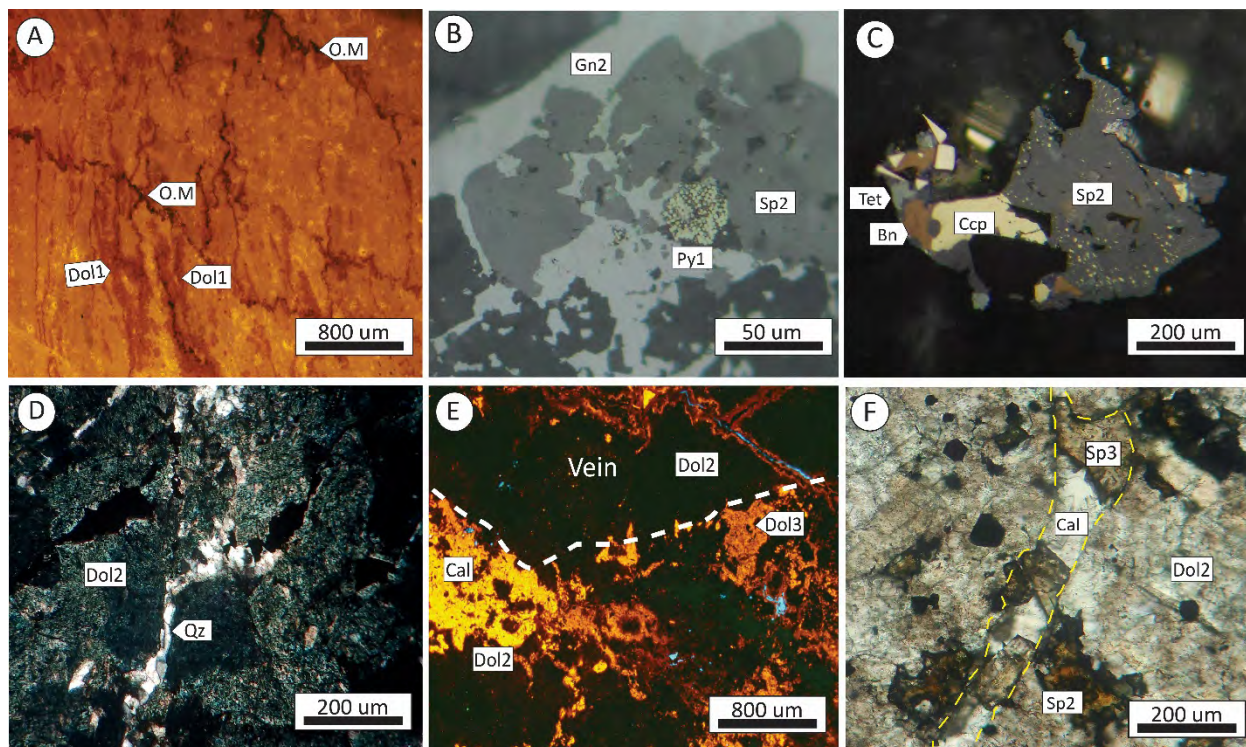
Figure 6 *: **A)** Cathodoluminescence photograph of central part of Kl that contains first generation dolomite around stylolite seam demarcated by organic matter. Dark orange areas, especially around organic matter in the stylolite, are first generation dolomite. **B)** Reflected light photomicrograph of galena, sphalerite and framboidal pyrite. Framboidal pyrite is partly replaced by second generation galena and sphalerite. **C)** Reflected light photomicrograph of sphalerite contain chalcopyrite inclusions. **D)** Cross-polarized light photomicrograph of second-generation dolomitization crosscut by quartz veinlet in uppermost Kl (Klsd). This polished thin section is stained a dark blue colour, indicative of its iron-rich composition. **E)** Cathodoluminescence photomicrograph of dolomitic vein and matrix. White dashed line demarcates boundary of coarsely crystalline dolomite and dolomitic matrix. **F)** Transmitted light photomicrograph of calcite vein containing sphalerite. This vein cuts second generation dolomite. O.M.: Organic Matter; Dol1: First generation dolomite; Cal: Calcite; Dol2: Second generation dolomite; Qz: Quartz vein; Dol3: Third generation dolomite; Sp3: Third generation sphalerite; Ccp: Chalcopyrite; Bn: Bornite; Tet: Tetrahedrite; Gn2: Second generation galena; Py1: First-generation pyrite.*

that these two deposits are misclassified. The presence of load casts and the occurrence of minute euhedral barite in the main ore horizon (uppermost part of the "Kl" ("Klsd")) in Eastern Haft-Savaran can be interpreted as indicating a syngenetic to syn-diagenetic origin.

Irish-type Pb-Zn mineralization in the Irish ore field occurs in non-argillaceous carbonates within mixed carbonate–siliciclastic successions formed in extensional tectonic environments (Hitzman & Beaty, 1996; Hitzman *et al.,* 2002; Wilkinson *et al.,* 2005; Wilkinson, 2003, 2014). Similar to Irish-type deposits, the Eastern Haft-Savaran deposit is hosted in limestone. The presence of micrite to biomicrite lithofacies (wackestone) in the "Kl" indicates formation under quiescent marine conditions (Folk, 1959; Wright, 1992). The micritic nature of "Kl", its gray to light gray colour, thick accumulation, and massive nature collectively indicate deposition on a deep shelf margin (Wilson, 1975; Alnaji, 2002). Organic matter-bearing gray micrite and wackestone lithofacies of limestone without clastic grains in the Kl unit indicate deposition in a low-energy marine environment. Unconsolidated carbonate sediments typically have 40 to 70 vol.% porosity (Choquette & Pray, 1970). Voids and pore spaces in carbonate sediments

can be formed during sedimentation and can be filled extensively with carbonate cement (Choquette & Pray, 1970) and ore-associated hydrothermal precipitates soon after burial. Although the porosity in unconsolidated carbonate sediments may have been preexisting, mineralizing solutions may have created additional porosity via their acidic nature. Both possibilities would have provided ideal conditions for the formation of large orebodies. Carbonate dissolution is maximized by moderately acidic (pH 4 to 5) fluids (Plumlee *et al.,* 1994). When combined with metalliferous and H_2S fluid mixing, carbonate dissolution provides ideal conditions for precipitation of Pb-Zn mineralization (Liu *et al.,* 2021). Geological and textural evidence can be used to infer the mode of sulphur transport to the mineralization site. The presence of sulphide mineralization within a hydrothermal conduit represented by quartz and dolomite veins-veinlets suggests that some sulphur was transported to the mineralization site by metalliferous hydrothermal fluid as H_2S, and sulphide minerals precipitated in response to pH buffering and cooling. However, the close association of sulphide minerals with organic matter, together with sulphur isotope data (Mahmoodi *et al*., unpublished data) indicate that the most sulphur was provided by thermal and bacterial reduction of pore water sulphate.

		First generation dolomite				Second generation dolomite				Third generation dolomite		
		N: 14				N: 14				N: 13		
	Min	Mean	Std	Max	Min	Mean	Std	Max	Min	Mean	Std	Max
Mn	0.02	0.22	0.08	0.30	0.70	1.20	0.30	1.50	0.15	0.30	0.10	0.50
Fe	0.30	1.01	0.50	1.90	7.50	8.32	0.40	9.02	1.02	2.00	0.60	3.06
Cu	0	0.17	0.30	0.80	0	0.01	0.01	0.03	0	0.03	0.08	0.30
Zn	0.01	0.05	0.03	0.10	0.01	0.05	0.04	0.16	0	0.01	0.01	0.02
Pb	0.01	0.02	0.10	0.04	0.01	0.04	0.02	0.10	0	0.01	0.05	0.01
Mg	6.40	8.70	0.90	9.80	6.60	7.20	0.30	7.97	10.15	11.58	1.00	13.36
Ca	24.05	24.90	0.60	25.70	18.30	19.60	0.60	20.6	22.72	25.43	1.40	27.70

Table 1: *Mineral chemistry of carbonate minerals in the Eastern Haft-Savaran deposit. All values are in wt%.*
(Std – Standard Deviation)

The presence of a synsedimentary fault that served as a hydrothermal fluid conduit is one of the most important characteristics in submarine hydrothermal deposits formed in sedimentary basins (Goodfellow *et al.,* 1993; Goodfellow, 2004, 2007; Goodfellow & Lydon, 2007; Wilkinson *et al.,* 2005; Wilkinson, 2014). An important characteristic of a synsedimentary normal fault is the difference in thickness of strata in the hanging wall relative to the footwall of the fault and the amount of down-drop. Synsedimentary faults can also serve as magma conduits for the emplacement of volcanic rocks. Mineralogical zoning in submarine hydrothermal deposits is typical, with high contents of Cu-bearing sulphides in or near the synsedimentary fault, and sphalerite and barite predominating at increasing distances from it (Goodfellow *et al.,* 1993; Goodfellow & Lydon, 2007; Wilkinson, 2014). Additionally, mineralization is thickest near the synsedimentary fault (Goodfellow & Lydon, 2007; Wilkinson, 2014). During orogenesis, the synsedimentary normal fault may reactivated as a reverse fault during compression, such as has been documented in the Malayer-Esfahan Metallogenic Belt (e.g. Irankuh district: Boveiri Konari *et al.,* 2017).

There are marked differences in mineralization from the southern part to the northern part of the Eastern Haft-Savaran deposit, including: 1) thickness of mineralization ("Klsd" thickness), which thins from the southern part of the Eastern Haft-Savaran deposit (near the reverse fault) to the northern part of the deposit; 2) intensity and style of alteration from the southern part to the northern part of the Eastern Haft-Savaran deposit, with intense, thick silicification alteration (in the southern part) to weak, narrow (in the northern part); 3) mineralogical zoning, with chalcopyrite and tetrahedrite near the aphyric rhyodacite flow in the southern part of the deposit, and barite with minor galena and sphalerite in the northern part. Collectively, this evidence indicates the reverse fault in the southern part of deposit was originally a synsedimentary normal fault that served as the conduit for the mineralizing fluid, and then subsequently was reactivated as a reverse fault during the Zagros orogeny (115 to 60Ma; Agard *et al.,* 2011).

The presence of load casts that are the result of a galena-sphalerite-pyrite-quartz band sinking into lime mud in the central part of the Eastern Haft-Savaran deposit indicate mineralization formed in unlithified lime mud during early diagenesis.

Textural relationships in the Eastern Haft-Savaran deposit provide further insight into the replacement process. Mineralization and hydrothermal alteration around organic matter in the middle part of "Kl" and relict fossils within uppermost Kl indicate that hydrothermal minerals replaced host limestone in the middle and uppermost "Kl" strata intensively and organic matter played an important role in trapping metal by providing H_2S by facilitating pore water sulphate reduction. Lenses and pseudobreccia fragments of first stage mineralization within second stage mineralization in the uppermost portion of "Kl" indicate that second stage mineralization replaced first stage mineralization.

Framboidal pyrite and minute euhedral barite are both common in submarine hydrothermal deposits (Kelley *et al.*, 2004; Gadd *et al.*, 2016; Magnall *et al.,* 2016; Gadd *et al.,* 2017). The size of Brt[1] grains and the replacement of Brt[1] in both Orbitolina fossils and in the matrix interstitial to fossil fragments, together with the restriction of Brt[1] to the mineralized horizon, and its association with Sp[1] and Gn[1] indicate a hydrothermal origin for Brt[1]. In the Eastern Haft-Savaran deposit, minute euhedral barite formed in lime mud, and subsequently was cut and replaced with microsparite as diagenesis progressed. The close association between framboidal pyrite, minute euhedral barite, sphalerite and galena indicates mineralization in the Eastern Haft-Savaran deposit formed in unconsolidated mud by sub-seafloor replacement during early diagenesis.

Lens-shaped chalcopyrite inclusions formed via replacement of high-Fe sphalerite by Cu-bearing fluids aided by consumption of Fe in the sphalerite structure (Bortnikov *et al.,* 1991; Nagase & Kojima, 1997). These chalcopyrite inclusions may reflect the increasing temperature of the mineralizing fluid.

Carbonate chemistry

Iron carbonate and Fe-rich dolomite are the most prevalent hydrothermal alteration style associated with SedEx deposits (Lydon, 1996). Iron-bearing carbonatization as siderite and ankerite is present in the Meggen (Sáez *et al.,* 2011; Velasco *et al*., 1998) and Rammelsberg (Large & Walcher, 1999) SedEx deposits in Germany. Extensive siderite and ferroan dolomite hydrothermal alteration also occur in the Jason SedEx deposit in the MacMillan Pass district, Selwyn Basin, Yukon, Canada (Turner, 1990).

High Fe and Mn contents in second-generation dolomite (associated with main mineralization) in the Eastern Haft-Savaran deposit are similar to what has been documented in other SedEx deposits such as Lady Loreta (Large & McGoldrick, 1998) and HYC deposits (Large *et al.,* 2000). The presence of manganese in Fe-bearing dolomite (Dol^2), the lack of Mn-oxide (manganite, pyrolusite and psilomelane) and the occurrence of massive barite away from the fluid conduit of the Eastern Haft-Savaran deposit indicate that the main stage mineralizing fluid was relatively more reduced (i.e., H_2S concentrations were probably higher than SO_4), compared to the other stages. Under reduced conditions, Mn is soluble, and precipitation of Mn oxides does not occur. Manganese as 2+ valence substitution occurs in Fe-bearing dolomite of the Lady Loreta deposit, Australia and has been used as a geochemical indicator for SedEx deposit exploration (Large & McGoldrick, 1998).

Conclusions

Based on the back-arc extensional tectonic setting of the Arak Mining District, massive carbonate host rock, mineralization control by stratigraphy, minor volcanism, load casts of mineralization in host rock, mineralogical zonation within the mineralization together with intensive replacement textures, the presence of minute euhedral barite and framboidal pyrites (and their textural evolution), and ferroan dolomite alteration attendant with main stage of mineralization, mineralization in the Eastern Haft-Savaran deposit formed as sub-seafloor replacements during early diagenesis.

Therefore, the Eastern Haft-Savaran deposit can be classified as an Irish -type deposit.

Acknowledgements

References

Agard, P., Omrani, J., Jolivet, L., & Mouthereau, F. (2005). Convergence history across Zagros (Iran): constraints from collisional and earlier deformation. *International Journal of Earth Sciences*, v. 94, 401-419.

Aghanabati, A. (1998). Major sedimentary and structural units of Iran (map). *Journal of Geosciences*, 29–30.

Aghanabati, A. (2004). Geology of Iran: Geological Survey of Iran, 600 p.

Akbari, Z. (2017). Model for the Genesis of Ahangaran Fe-Pb Deposit (SE of Malayer), Based on Ore Types, Geochemistry and Stable (Shahid Beheshty University unpublished PhD thesis). pp. 311.

Akbari, Z., Yarmohammadi, A., & Rassa, I. (2020). Ore types, Structure, Texture, Mineralogy and Genesis of Ahangaran Fe-Pb Deposit, Southeast of Malayer, (Malayer-Esfahan metallogenic belt). *Scientific Quarterly Journal of Geosciences*, 29(116), 161-172.

Alavi, M. (1996). Tectonostratigraphic synthesis and structural style of the Alborz mountain system in northern Iran. *Journal of Geodynamics*, 21(1), 1-33.

Allen, M. B., & Armstrong, H. A. (2008). Arabia–Eurasia collision and the forcing of mid-Cenozoic global cooling. *Palaeogeography, Palaeoclimatology, Palaeoecology*, 265(1-2), 52-58.

Babakhani, A., Samimi, M.N., & Molaali, A.H. (1988). Geological studies on the Mehdiabad lead and zinc project: Geological Survey of Iran, unpublished internal report

Bagheri, S., & Stampfli, G. M. (2008). The Anarak, Jandaq and Posht-e-Badam metamorphic complexes in central Iran: new geological data, relationships and tectonic implications. *Tectonophysics,* 451(1-4), 123-155.

Berberian, M., & King, G. C. P. (1981). Towards a paleogeography and tectonic evolution of Iran. *Canadian journal of earth sciences*, 18(2), 210-265.

Bond, D.P.G. & Wignall, P.B., (2010) Pyrite framboid study of marine Permian–Triassic boundary sections: A complex anoxic event and its relationship to contemporaneous mass extinction. *Geological Society of America Bulletin* 122, 1265–1279.

Bottrell, S. H., & Newton, R. J. (2006). Reconstruction of changes in global sulfur cycling from marine sulfate isotopes. *Earth-Science Reviews*, 75(1-4), 59-83.

Boveiri, K. M., Rastad, E., Mohajjel, M., Nakini, A., & Haghdoost, M. (2015). Structure, texture, mineralogy and genesis of sulphide ore facies in Tappeh Sorkh detrital carbonate-hosted Zn-Pb (Ag) deposits, South of Esfahan. J. *Geosci.*, 221.

Boveiri, M. (2016). Ore-bearing Sulphide Facies and Genetic Model of Detrital-Carbonate Hosted Zn-Pb Mineralization in the Tappehsorkh Deposit, Irankuh Mining District, South Esfahan (Unpublished Ph.D thesis). Tarbiat Modares University, Tehran, Iran, pp. 415.

Boveiri, M., & Rastad, E. (2018). Nature and origin of dolomitization associated with sulphide mineralization: new insights from the Tappehsorkh Zn-Pb (-Ag-Ba) deposit, Irankuh Mining District, Iran. *Geological Journal,* v. 53(1), 1-21.

Boveiri, M., Rastad, E., & Peter, J. M (2017). A sub-seafloor hydrothermal syn-sedimentary to early diagenetic origin for the Gushfil Zn-Pb-(Ag-Ba) deposit, south Esfahan, Iran. *Journal of Mineralogy and Geochemistry*, v. 194, 61-90.

Canfield, D. E., Farquhar, J., & Zerkle, A. L. (2010). High isotope fractionations during sulfate reduction in a low-sulfate euxinic ocean analog. *Geology*, v. 38(5), 415-418.

Deb, M., & Goodfellow, W. D. (2004). Sediment Hosted Lead-Zinc Sulphide Deposits. CRC Press.

Ehya, F., & Marbouti, Z. (2021). The Shamsabad Fe-Mn deposit, Markazi province, Iran: LA-ICP-MS and sulfur isotopic geochemistry. *Ore Geology Reviews,* v. 139, 104555.

Ehya, F., Lotfi, M., & Rasa, I. (2010). Emarat carbonate-hosted Zn–Pb deposit, Markazi Province, Iran: A geological, mineralogical and isotopic (S, Pb) study. *Journal of Asian Earth Sciences*, v. 37(2), 186-194.

Ghasemi, A., & Talbot, C. J. (2006). A new tectonic scenario for the Sanandaj–Sirjan Zone (Iran). *Journal of Asian Earth Sciences*, v. 26(6), 683-693.

Ghasemi, M. (2006). Formation mechanism of the Mehdiabad Zn–Pb deposit and its comparison with other near lead and zinc deposits

[Unpublished M.Sc. thesis]: Research Institute of Earth Sciences, Geological Survey of Iran, 238 p.

Ghazban, F., McNutt, R. H., & Schwarcz, H. P. (1994). Genesis of sediment-hosted Zn-Pb-Ba deposits in the Irankuh district, Esfahan area, west-central Iran. *Economic Geology,* v. 89(6), 1262-1278.

Golonka, J. (2004). Plate tectonic evolution of the southern margin of Eurasia in the Mesozoic and Cenozoic. *Tectonophysics*, v. 381(1-4), 235-273.

Han, C., Song, Y., Liu, Y., Hou, Z., Cheng, Y., & Zhai, Z. (2020). Characteristics and genesis of the Ahangaran Pb Cu deposit Iran. *Geological Bulletin of China,* v. 39(10), 1625-1638.

Horton, B. K., Hassanzadeh, J., Stockli, D. F., Axen, G. J., Gillis, R. J., Guest, B. & Grove, M. (2008). Detrital zircon provenance of Neoproterozoic to Cenozoic deposits in Iran: Implications for chronostratigraphy and collisional tectonics. *Tectonophysics*, v. 451(1-4), 97-122.

Hosseini-Dinani, H., & Aftabi, A. (2016). Vertical lithogeochemical halos and zoning vectors at Goushfil Zn–Pb deposit, Irankuh district, southwestern Isfahan, Iran: Implications for concealed ore exploration and genetic models. *Ore Geology Reviews*, v. 72, 1004-1021.

Jørgensen, B. B., Isaksen, M. F., & Jannasch, H. W. (1992). Bacterial sulfate reduction above 100 C in deep-sea hydrothermal vent sediments. *Science*, v. 258(5089), 1756-1757.

Karimpour, M. H., & Sadeghi, M. (2018). Dehydration of hot oceanic slab at depth 30–50 km: KEY to formation of Irankuh-Emarat PbZn MVT belt, Central Iran. *Journal of Geochemical Exploration*, v. 194, 88-103.

Karimpour, M. H., Malekzadeh Shafaroudi, A., Esmaeili Sevieri, A., Saeed, S., Allaz, J. M., & Stern, C. R. (2017). Geology, mineralization, mineral chemistry, and ore-fluid conditions of Irankuh Pb-Zn mining district, south of Isfahan. *Journal of Economic Geology*, v. 9(2), 267-294.

Kiyosu, Y., & Krouse, H. R. (1990). The role of organic acid in the abiogenic reduction of sulfate and the sulfur isotope effect. *Geochemical Journal*, v. 24(1), 21-27.

Leach, D. L., Bradley, D. C., Huston, D., Pisarevsky, S. A., Taylor, R. D., & Gardoll, S. J. (2010). Sediment-hosted lead-zinc deposits in Earth history. *Economic Geology,* v. 105(3), 593-625.

Leach, D. L., Sangster, D. F., Kelley, K. D., Large, R. R., Garven, G., Allen, C. R. & Walters, S. (2005). Sediment-hosted lead-zinc deposits: A global perspective. *Economic Geology*, vol. 100th , pp. 561-607 .

Lowenstein, T. K., Hardie, L. A., Timofeeff, M. N., & Demicco, R. V. (2003). Secular variation in seawater chemistry and the origin of calcium chloride basinal brines. *Geology*, v. 31(10), 857-860.

Maanijou, M., Fazel, E. T., Hayati, S., Mohseni, H., & Vafaei, M. (2020). Geology, fluid inclusions, C–O–S–Pb isotopes and genesis of the Ahangaran Pb-Ag (Zn) deposit, Malayer-Esfahan Metallogenic Province, western Iran. *Journal of Asian Earth Sciences*, v. 195, 104339.

Maghfouri, S., Hosseinzadeh, M. R., Choulet, F., Alfonso, P., Zadeh, A. M. A., & Rajabi, A. (2019). Vent-proximal sub-seafloor replacement clastic-carbonate hosted SEDEX-type mineralization in the Mehdiabad world-class Zn-Pb-Ba-(Cu-Ag) deposit, southern Yazd Basin, Iran. *Ore Geology Reviews*, v. 113, 103047.

Mahmoodi, P. (2018). Ore Facies, Geology and Geochemistry of Haftsavaran and Hosseinabad Zn-Pb deposits, Malayer-Esfahan Metallogenic Belt. PhD Thesis. Tarbiat Modares University.

Mahmoodi, P., Rastad, E., Rajabi, A., & Moradpour, M. (2019). Mineralization horizons, structure and texture, alteration and mineralization stages in the Zn-Pb (Ba) Eastern Haft-Savaran deposit in Malayer-Esfahan metallogenic belt, south of Khomain. *Scientific Quarterly Journal of Geosciences*, v. 28(110), 3-12.

Mahmoodi, P., Rastad, E., Rajabi, A., & Moradpour, M. (2019). Mineralization horizons, stracture and texture, alteration and mineralization stages in the Zn-Pb (Ba) Eastern Haft-Savaran deposit in Malayer-Esfahan metallogenic belt, south of Khomain. *Scientific Quarterly Journal of Geosciences*, v. 28(110), 3-12.

Mahmoodi, P., Rastad, E., Rajabi, A., & Peter, J. M. (2018). Ore facies, mineral chemical and fluid inclusion characteristics of the Hossein-Abad and Western Haft-Savaran sediment-hosted Zn-Pb deposits, Arak Mining District, Iran. *Ore Geology Reviews*, v. 95, 342-365.

Mahmoodi, P., Rastad, E., Rajabi, A., Alfonso, P., Canet, C., & Peter, J. M. (2021). Genetic model for Jurassic shale-hosted Zn-Pb deposits of the Arak Mining District, Malayer-Esfahan metallogenic belt: Insight from sedimentological, textural, and stable isotope characteristics. *Ore Geology Reviews*, v. 136, 104262.

Moghadam, H. S., Whitechurch, H., Rahgoshay, M., & Monsef, I. (2009). Significance of Nain-Baft ophiolitic belt (Iran): Short-lived, transtensional Cretaceous back-arc oceanic basins over the Tethyan subduction zone. *Comptes Rendus Geoscience,* v. 341(12), 1016-1028.

Mohajjel, M., & Fergusson, C. L. (2014). Jurassic to Cenozoic tectonics of the Zagros Orogen in northwestern Iran. *International Geology Review*, v. 56(3), 263-287.

Momenzadeh, M. (1976). Stratabound lead–zinc ores in the Lower Cretaceous and Jurassic sediments in the Malayer–Esfahan district (west central Iran), lithology, metal content, zonation and genesis. Heidelberg, PhD Thesis, University of Heidelberg, 300pp.

Movahednia, M., Rastad, E., Rajabi, A., Maghfouri, S., González, F. J., Alfonso, P. & Canet, C. (2020). The Ab-Bagh Late Jurassic-Early Cretaceous sediment-hosted Zn-Pb deposit, Sanandaj-Sirjan zone of Iran: Ore geology, fluid inclusions and (S–Sr) isotopes. *Ore Geology Reviews*, v. 121, 103484.

Nakini, A. (2013). The Structural Analysis of Irankuh and Tiran Areas (S and W Isfahan) (Unpublished M.Sc. thesis). Tarbiat Modares University, Tehran, pp. 182.

Niroomand, S., Haghi, A., Rajabi, A., Shabani, A. A. T., & Song, Y. C. (2019). Geology, isotope geochemistry, and fluid inclusion investigation of the Robat Zn-Pb-Ba deposit, Malayer-Esfahan metallogenic belt, southwestern Iran. *Ore Geology Reviews*, v. 112, 103040.

Peernajmodin, H. (2018). Ore Facies, Geology and Geochemistry of Khanabad, Shamsabad and Kuhkolangeh Zn-Pb and Fe deposits, Malayer-Esfahan Metallogenic Belt. PhD Thesis. Tarbiat Modares University.

Peernajmodin, H., Rastad, E., & Rajabi, A. (2018). Ore structural, textural, mineralogical and fluid inclusions studies of the Kouh-Kolangeh Zn-Pb-Ba deposit, Malayer-Isfahan metallogenic belt, South Arak, Iran. *Scientific Quarterly Journal of Geosciences*, v. 27(107), 287-302.

Rajabi, A. (2022). Metallogeny and geology of sediment-hosted Zn-Pb deposits of Iran. University of Tehran Press. 470 pp.

Rajabi, A., Alfonso, P., Canet, C., Rastad, E., Niroomand, S., Modabberi, S., & Mahmoodi, P. (2020). The world-class Koushk Zn-Pb deposit, Central Iran: A genetic model for vent-proximal shale-hosted massive sulfide (SHMS) deposits–Based on paragenesis and stable isotope geochemistry. *Ore Geology Reviews,* v. 124, 103654.

Rajabi, A., Canet, C., Alfonso, P., Mahmoodi, P., Yarmohammadi, A., Sharifi, S. & Rezaei, S. (2022). Mineralization and Structural Controls of the AB-Bid Carbonate-Hosted Pb-Zn (±Cu) Deposit, Tabas-Posht e Badam Metallogenic Belt, Iran. *Minerals*, v. 12(1), 95.

Rajabi, A., Canet, C., Rastad, E., & Alfonso, P. (2015). Basin evolution and stratigraphic correlation of sedimentary-exhalative Zn–Pb deposits of the Early Cambrian Zarigan–Chahmir Basin, Central Iran. *Ore Geology Reviews*, v. 64, 328-353.

Rajabi, A., & Mahmoodi, P., (2023). Metallogeny of Sediment-Hosted Zinc-Lead (SH Zn-Pb) Deposits of Iran. 2nd annual conference on Iranian Mineral deposits, 2022 - Conference on Iranian Pb-Zn deposits.

Rajabi, A., Mahmoodi, P., Rastad, E., Niroomand, S., Canet, C., Alfonso, P., Tabakh Shabani, A., & Yarmohammadi, A. (2019a). Comments on "Dehydration of hot oceanic slab at depth 30–50 km: Key to formation of Irankuh-Emarat Pb-Zn MVT belt, Central Iran" by Mohammad Hassan Karimpour and Martiya Sadeghi. *Journal of Geochemical Exploration*, v. 205, 106346.

Rajabi, A., Mahmoodi, P., Rastad, E., Niroomand, S., Peernajmodin, H., Akbari, Z., Fadaei, M.J., Yarmohammadi, A., Movahednia, M., Azizzadeh, B., & Haghi, A. (2019b). A review of fluid inclusion investigations on Cretaceous sediment-hosted Zn-Pb (± Ba ± Fe ± Ag ± Cu) deposits in the Malayer-Esfahan metallogenic belt (MEMB). Third Biennial Iranian National Fluid Inclusion conference.

Rajabi, A., Rastad, E., & Canet, C. (2012a). Metallogeny of Cretaceous carbonate-hosted Zn–Pb deposits of Iran: geotectonic setting and data integration for future mineral exploration. *International Geology Review,* v. 54(14), 1649-1672.

Rajabi, A., Rastad, E., & Canet, C. (2013). Metallogeny of Permian–Triassic carbonate-hosted Zn–Pb and F deposits of Iran: a review for future mineral exploration. *Australian Journal of Earth Sciences*, v. 60(2), 197-216.

Rajabi, A., Rastad, E., Alfonso, P., & Canet, C. (2012b). Geology, ore facies and sulphur isotopes of the Koushk vent-proximal sedimentary-exhalative deposit, Posht-e-Badam Block, Central Iran. *International Geology Review*, v. 54(14), 1635-1648.

Rajabi, A., Rastad, E., Canet, C., & Alfonso, P. (2015b). The Early Cambrian Chahmir shale-hosted Zn–Pb deposit, Central Iran: an example of vent-proximal SEDEX mineralization. *Mineralium Deposita*, 50, 571-590.

Rastad, E. (1981). Geological, mineralogical, and facies investigations on the Lower Cretaceous stratabound Zn–Pb–(Ba–Cu) deposits of the Iran Kouh Mountain Range, Esfahan, west Central Iran [Unpublished Ph.D. thesis]: Heidelberg, University of Heidelberg, 334 p.

Reichert, J. (2007). A metallogenetic model for carbonate-hosted non-sulphide zinc deposits based on observations of Mehdi Abad and Irankuh, Central and Southwestern Iran. (unpublished PhD thesis, Martin-Luther-Universität Halle-Wittenberg,

Wilkin, R.T., Barnes, H.L., & Brantley, S.L. (1996) The size distribution of framboidal pyrite in modern sediments: An indicator of redox conditions. *Geochimica et Cosmochimica Acta,* v. 60, 3897–3912**.**

Wilkinson, J. J. (2014). Sediment-Hosted Zinc-Lead Mineralization: Processes and Perspectives: Processes and Perspectives. *Geology, 2013*

Yarmohammadi, A. (2015). Origin and Characteristics of Ore Forming Fluids and Genetic Model of Carbonate Hosted Zn-Pb Deposits in Upper Part of Lower Cretaceous Sequence, North Tiran Basin in NW of Esfahan (Unpublished Ph.D. thesis). Tarbiat Modares University, Tehran, pp. 395

Yarmohammadi, A., Rastad, E., & Rajabi, A. (2016). Geochemistry, fluid inclusion study and genesis of the sediment-hosted Zn-Pb (±Ag±Cu) deposits of the Tiran basin, NW of Esfahan, Iran. *Journal of Mineralogy and Geochemistry,* v. 193, 183-203.